Fracture Mechanics of Concrete Structures, de Borst et al (eds) © 2001 Swets & Zeitlinger, Lisse, ISBN 90 2651 825 0

Cracking of R/C tensile members reinforced by FRP-plates

D. Ferretti
Department of Civil Engineering, University of Parma, Italy
M.Savoia
Distart – Structural Engineering, University of Bologna, Italy

ABSTRACT: The role of FRP-composite plates for strengthening of reinforced concrete structural elements subjected to axial loads is analyzed, with particular emphasis to the evolution of crack pattern and its consequences on tensile deformability. A non-linear model is developed, where cohesive stresses in concrete across cracks, non-linear bond-slip between steel bars and concrete, and linear constitutive laws at the concrete-FRP interface are considered. The non-linear governing equations are solved via finite difference method. A numerical example is presented, simulating a test with displacement control on a plated and an unplated reinforced concrete member, where the evolution of the crack pattern along the tensile member is followed. The example confirms that external FRP-plating can be effective in reducing crack width and, consequently, in increasing stiffness of tensile members. This is mainly due to the fact that the transfer length of bond-slip phenomenon at the concrete-plate interface is significantly smaller than the concrete-steel bar counterpart.

1 INTRODUCTION

External plating by means of Carbon or Glass Fiber Reinforced Plastics (FRP) plates or sheets is one of the most promising and efficient reinforcement techniques for axial, bending or shear strengthening of reinforced concrete (R/C) elements. FRP reinforcement is considered effective both in increasing ultimate loading and in reducing deformability due to crack opening.

Nevertheless, in spite of the significant increasing number of applications of this strengthening technique in common engineering practice, a lack of information can be registered as far as reliable theoretical models and experimental results are concerned. In literature several studies can be found on the ultimate behavior of reinforced concrete beams strengthened by external plates in standard conditions (e.g. Saadatmanesh & Ehsani 1991, Nanni 1993, Varastehpour & Hamelin 1997). On the contrary, only a few studies concern their serviceability behavior. Moreover, some important local phenomena (related to the complexity of concrete-FRP interface mechanism) have not been sufficiently investigated up to date, even though they represent the principal mechanisms of structural failure (Jones et al. 1988, Malek et al. 1998, Garden & Quantrill 1998).

Local phenomena should be understood in order to obtain a correct evaluation of safety margins of rehabilitation design with respect to ultimate and serviceability limit states.

As far as theoretical studies are concerned, solutions based on simple shear-lag models (as initially proposed by Volkersen 1938), are not in general sufficiently accurate. Neglecting bending of bonded plates, shear-lag models do not allow to compute the so-called secondary stresses, such as the peeling stress, which are often very important since they can represent the onset of plate debonding.

To evaluate primary and secondary stresses, concrete element and composite plate have been modelled as beams linked by the layer of glue (e.g. Bresson 1971, Roberts 1989a, b, Taljsten 1997a). Usually, these linear-elastic models are devoted only to the analysis of stresses close to FRP-plate extremities. Recently, Ferretti & Savoia (2000) analyzed the stress state close to a transverse crack in a R/C tensile member. Their study showed that, as stiffness of concrete-plate interface is higher than concrete-steel counterpart, strain in FRP-plate could even be three times greater than steel strain. As a consequence, classical hypothesis of plane strain profile, typically used for design purposes (see for instance FIB TG 4.2 1999, JSCE 1997), should be rediscussed.

For this reason, in the present study a non-linear model is developed to study the evolution of crack pattern in R/C tensile members retrofitted by FRP plates.

In transversal cracks, non-linear behavior is taken into account by means of cohesive stresses, which

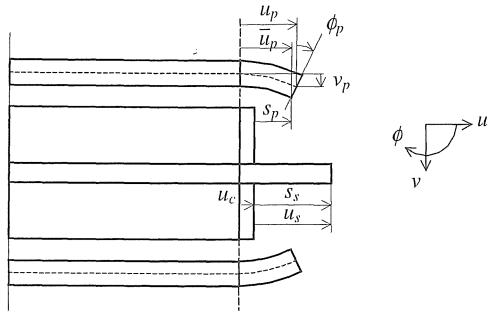

Figure 1. Kinematic hypotheses and definition of slip between plate, concrete, and steel.

play a significant role due to small crack width.

Non-linear bond-slip relationship between reinforcing steel and concrete is considered. Finally, at concrete-FRP interface linear constitutive laws are adopted. This choice is supported by the fact that peeling cracks have never been observed in the neighborhood of transverse cracks in concrete, so that no damage is introduced.

The non-linear governing differential equations are solved via Finite Difference Method (FDM) in the case of force as well as displacement control.

An illustrative numerical example is presented where the evolution of crack pattern is followed and different behaviors of plated and unplated members are compared. The examples show that the characteristic length of bond-slip phenomenon between concrete and composite plate is significantly shorter than the concrete-steel bar counterpart, so that external plating is very effective in reducing crack width and, consequently, in increasing stiffness in the cracked stage.

2 NONLINEAR MODEL FOR FRP-REINFORCED TENSILE MEMBERS

2.1 *Kinematics*

A displacement-based model is formulated for a R/C tensile member reinforced along its length by a symmetric couple of composite FRP plates.

Transverse cross-section of the concrete element is assumed to remain plane after deformation. Hence, concrete and steel bars are subject to axial deformations only, denoted by ε_c and ε_s, respectively. Moreover, Bernoulli beam theory is adopted for the composite plates (i.e. shear deformations are neglected), with ε_p and φ_p denoting axial strain of the middle plane and rotation of the transverse cross-section. The notation adopted for kinematic components is reported in Figure 1. Subscripts *c*, *s* and *p* denote quantities related to concrete, steel bars and composite plates, respectively. Relative displacements between different constituents are considered (see Fig. 2). In particular, at the concrete-steel interface, tangential slip is defined as the difference of displacements $s_s = u_s - u_c$ of two points belonging to steel and concrete which were initially in contact. At the concrete-plate interface both tangential and normal relative displacements are considered. Tangential slip is defined as:

$$s_p = \bar{u}_p - u_c = u_p - \varphi_p \frac{h_p}{2} - u_c , \tag{1}$$

where u_p = displacement of the surface of the glued plate; h_p = plate thickness.

Normal relative displacement between concrete and plate coincides with the plate transverse displacement v_p.

As far as the interface laws are concerned, according to the notations depicted in Figures 1 and 2, concrete – steel constitutive law can be written in the general form:

$$\tau_s = -f_s(s_s) . \tag{2}$$

The general equations written for the concrete-plate interface

$$\tau_p = -f_t(s_p , v_p) , \tag{3a}$$

$$\sigma_v = -f_n(s_p, v_p) , \tag{3b}$$

consider the coupling between tangential and transverse normal stresses which is evident, as will be discussed in Section 3.3, when interface microcracking occurs.

If, for the sake of simplicity, uncoupling between tangential and normal laws for concrete-plate interface is assumed, Equations 2, 3 can be expressed as:

$$\tau_s = -k_s(s_s)\, s_s , \tag{4}$$

$$\tau_p = -k_{pu}(s_p)\, s_p , \tag{5a}$$

$$\sigma_v = -k_{pv}(v_p)\, v_p , \tag{5b}$$

where $k_s(s_s)$, $k_{pu}(s_p)$, $k_{pv}(v_p)$ are secant stiffnesses. The introduction of secant stiffnesses allows for the use of classical numerical techniques for the solution of non-linear problem.

2.2 *Equilibrium and compatibility equations*

The notation adopted for stress resultants is reported in Figure 2 with reference to a free body diagram of infinitesimal length. Making use of Equations 5a, b the equilibrium conditions for the differential composite plate element are:
where $K_{pu}=b_p k_{pu}$, and $K_{pv}=b_p k_{pv}$ are the secant interface stiffnesses.

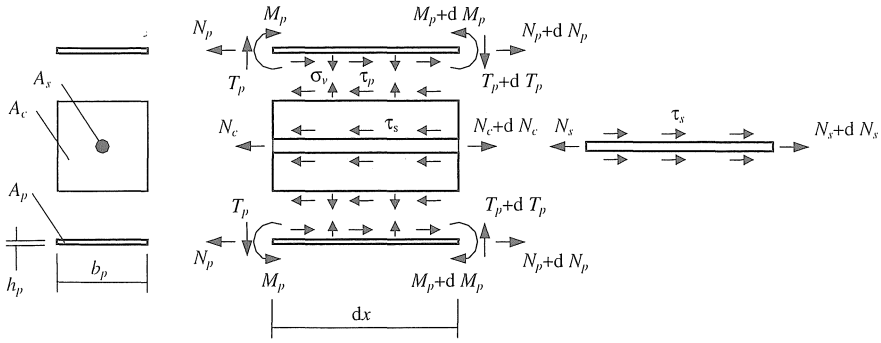

Figure 2. Free body diagram of an infinitesimal portion of tensile member.

$$\frac{\mathrm{d}N_p}{\mathrm{d}x} = -b_p \tau_p = K_{pu} s_p \ , \tag{6}$$

$$\frac{\mathrm{d}T_p}{\mathrm{d}x} = -b_p \sigma_v = K_{pv} v_p \ , \tag{7}$$

$$\frac{\mathrm{d}M_p}{\mathrm{d}x} = T_p - \tau_p \frac{h_p}{2} b_p = T_p - \frac{h_p}{2} K_{pu} s_p \ , \tag{8}$$

Moreover, assuming a linear behavior for composite plate, Euler-Bernoulli theory gives the following compatibility differential equations:

$$\frac{\mathrm{d}u_p}{\mathrm{d}x} = \frac{N_p}{E_p A_p} - \frac{M_p h_p}{2 E_p J_p} , \tag{9}$$

$$\frac{\mathrm{d}v_p}{\mathrm{d}x} = \varphi_p , \tag{10}$$

$$\frac{\mathrm{d}\varphi_p}{\mathrm{d}x} = -\frac{M_p}{E_p J_p} . \tag{11}$$

where A_p, J_p, E_p stand for area, moment of inertia and Young modulus of the composite plate.

Furthermore, compatibility and equilibrium equations for concrete and steel bar are:

$$\frac{\mathrm{d}u_c}{\mathrm{d}x} = \frac{N_c}{E_c A_c} , \tag{12}$$

$$\frac{\mathrm{d}N_c}{\mathrm{d}x} = -K_s (u_s - u_c) + 2K_{pu} (u_c + \varphi_p \frac{h_p}{2} - u_p) , \tag{13}$$

$$\frac{\mathrm{d}u_s}{\mathrm{d}x} = \frac{N_s}{E_s A_s} , \tag{14}$$

$$\frac{\mathrm{d}N_s}{\mathrm{d}x} = K_s (u_s - u_c) , \tag{15}$$

where K_s=$n_p \pi \Phi k_s$, n_b = number of steel bars and Φ = diameter of steel bars.

3 CONSTITUTIVE AND INTERFACE LAWS

3.1 *Uniaxial behavior of concrete in tension*

The behavior of concrete in tension is assumed to be linear elastic, with modulus of elasticity E_c equal to the initial tangent modulus in compression, up to tensile strength f_{ct}. When tensile strength is reached, a transversal crack appears. Then, fictitious crack model is used to define the cohesive tensile stresses in concrete σ_{ct} as a function of the fictitious crack opening w. Cohesive tensile stresses are particularly significant for plated members because of the narrow crack width.

When a new transversal crack arises and grows, partial closure of previously formed cracks occurs especially in a displacement-controlled test. Therefore, both loading and unloading curves are introduced according to the cyclic model proposed by Hordijk (1992).

3.2 *Steel-concrete bond-slip laws*

Bond behavior between reinforcing steel and concrete is modeled by extending the classical simplified bond-slip relationship proposed in CEB-FIP (1992). Also in this case, cyclic laws are required since, when a new crack arises, reduction of axial load causes unloading of steel concrete interface, with slips that in some cases may also reverse their sign. Cyclic loading produces a progressive deterioration of steel-concrete bond, which is taken into account according to Eligehausen et al. (1983).

For the sake of simplicity, the reduced bond resistance close to free surfaces (member ends and transverse cracks) due to the reduced boundary restraint is not considered here. This hypothesis is acceptable close to transverse cracks for plated members because, due to plating, the crack width is small. In addition, plates provide for a significant confinement also in the transversal direction.

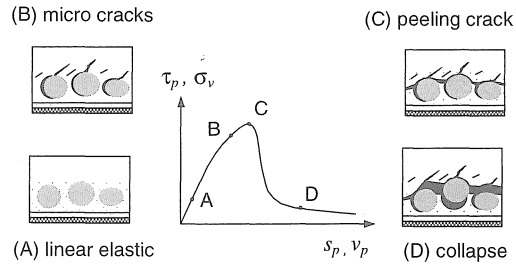

Figure 3. Plate – concrete interface behavior: influence of damage on plate – concrete interface laws.

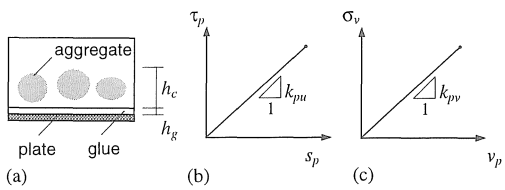

Figure 4. Plate – concrete interface behavior: (a) layer of concrete aggregates anchored in the film of glue; linear (b) bond – slip law and (c) normal stress – displacement law adopted in the present analysis.

3.3 *Plate-concrete interface laws*

In the last years, several researches considered the problem of concrete-plate interface laws.

At the beginning, experimental studies were devoted only to the estimate of minimum anchor length for efficient force transfer and maximum transmissible axial force (Bresson 1971, Ranisch 1982). These tests did not provide measurements of local strains in the plates, so that they cannot be used to derive a local interface constitutive law.

More recently, experimental tests have been performed, based on pull-out, single-lap, and double-lap tests (Swami et al. 1986, Chajes et al. 1996, Taljsten 1997b, Lee et al. 1999, Tripi et al. 2000), half-beam specimens (Ziraba et al. 1995), or more complex experimental setups (Volnyy & Pantelides 1996). Axial strains along the plate have been measured, so giving the possibility of deriving average interface shear stresses, i.e. average values between two consecutive strain gauges. Nevertheless, the difficulties in conducting the tests reduce considerably the significance of the results. In fact, bond and force transfer mechanisms are confined in small portions of the joints (few centimeters), where many strain gauges must be placed to measure the steep decay of strains along the plate. Moreover, the axial strains measured on the external face of the plate are influenced by plate bending, which is very difficult to be avoided especially when interface failure takes place. Finally, when micro-cracks in a thin layer of the concrete substrate propagate and coalesce in macro-cracks, bond-slip τ_p–s_p and normal stress-displacement σ_v–v_p relationships cannot be longer considered as uncoupled.

Hence, due to the complexity of the problem, experimental tests and theoretical models on concrete-plate interface are usually based on the interface tangential stress-strain τ_p–s_p relationship only (e.g. Hankers & Rostásy 1997, Brosens & Van Gemert 1998, Jansze 1997).

Tests showed that a layer of concrete aggregates anchored in the film of glue participates to bond behavior. According to Brosens & van Gemert (1998), the thickness h_c of this layer is related to maximum aggregate size and concrete external cover. For low loading levels, glue and concrete cover exhibit an approximately linear elastic behavior (point *A* in Fig. 3), so that constitutive interface laws can be expressed as:

$$\tau_p = \frac{1}{h_g/G_g + h_c/G_c} s_p = k_{pu} s_p \,, \tag{16}$$

$$\sigma_v = \frac{1}{h_g/E_g + h_c/E_c} v_p = k_{pv} v_p \,, \tag{17}$$

where G_g, E_g and G_c, E_c are the shear and Young moduli of glue and concrete, respectively (Fig. 4).

For increasing values of relative displacements s_p and v_p between concrete and plate, microcracks start growing at the concrete-plate interface and propagating in the concrete substrate. Therefore, the two laws exhibit a non-linear behavior (point *B* in Fig. 3) until interface failure. The peak stress (point *C*) is reached when microcracks coalesce giving rise to a macro crack, called peeling crack (Hankers 1995).

Usually a concrete failure criterion (e.g. Mohr-Coulomb criterion) is used to detect the onset of a peeling crack, starting from principal stresses. However, due to the very steep variation of peeling stresses along the plate axis (from the maximum value at the plate end to zero in about 10÷15 mm), principal stresses computed in one point can be not fully representative of physical evidence. Non-local failure criteria are then probably more appropriate.

When peeling crack appears, load transferring capacity of the interface drops drastically producing a softening behavior in both laws, with stresses depending both on crack slip and crack width (point *D* in Fig. 3).

Unfortunately, the available experimental data are not enough at the present to calibrate the softening branch of non-linear constitutive laws. Therefore, in the present analysis, linear behavior according to Equations 16, 17 is assumed. This hypothesis seems acceptable if the analysis is limited to serviceability range.

4 NUMERICAL SOLUTION VIA FINITE DIFFERENCE METHOD

The system of governing differential Equations 4-8 is rewritten in the compact form:

$$\mathbf{y}'(x) = \mathbb{A}(\mathbf{y}, x)\,\mathbf{y}(x) \qquad 0 \le x \le L, \tag{18}$$

where $\mathbf{y}$ is the vector collecting the unknowns stress resultants and displacements

$$\mathbf{y}^T = \left\{N_s, N_p, N_c, M_p, T_p, u_s, u_p, u_c, v_p, \varphi_p\right\}. \tag{19}$$

The boundary conditions defined at the two ends $x = 0, L$ of the member can be written as:

$$\mathbb{B}_a\,\mathbf{y}(0) + \mathbb{B}_b\,\mathbf{y}(L) = \mathfrak{a}\,. \tag{20}$$

Vector $\mathfrak{a}$ takes different forms if the axial force N or axial elongation ΔL is prescribed, to simulate tests with force or displacement control, respectively. The extended form for matrices $\mathbb{A}(\mathbf{y}, x)$, $\mathbb{B}_a$, $\mathbb{B}_b$ and vector $\mathfrak{a}$ are reported in Ferretti & Savoia (2000).

Equations 18, 20 represent a nonlinear boundary value problem that can be solved via finite difference method.

Following the algorithm proposed in Ascher et al. (1988), the interval [0, L] is divided in J nodes at uniform distance h, $0 = x_0 < x_1 < \ldots < x_J = L$.

For the general j-th interior mesh point ($0 < j < J$), the derivative in Equation 18 is replaced by the central finite difference approximation $(\mathbf{y}_{j+1} - \mathbf{y}_j)/h$ centered at $x_{j+1/2}$. Finite difference equations, together with boundary conditions, lead to the non-linear system:

$$\begin{vmatrix} \mathbb{S}_1 & \mathbb{R}_1 & & & & & \\ & \mathbb{S}_2 & \mathbb{R}_2 & & & & \\ & & \ldots & \ldots & & & \\ & & & \mathbb{S}_j & \mathbb{R}_j & & \\ & & & & \ldots & \ldots & \\ & & & & & \mathbb{S}_J & \mathbb{R}_J \\ \mathbb{B}_a & & & & & & \mathbb{B}_b \end{vmatrix} \begin{vmatrix} \mathbf{y}_0 \\ \mathbf{y}_1 \\ \ldots \\ \mathbf{y}_j \\ \ldots \\ \mathbf{y}_{J-1} \\ \mathbf{y}_J \end{vmatrix} = \begin{vmatrix} \mathbf{0} \\ \mathbf{0} \\ \ldots \\ \mathbf{0} \\ \ldots \\ \mathbf{0} \\ \mathfrak{a} \end{vmatrix}, \tag{21}$$

where:

$$\mathbb{S}_j = -\frac{1}{h}\mathbb{I} - \frac{1}{2}\mathbb{A}(\mathbf{y}_j, x_j), \tag{22}$$

$$\mathbb{R}_j = +\frac{1}{h}\mathbb{I} - \frac{1}{2}\mathbb{A}(\mathbf{y}_{j+1},\ x_{j+1}) \quad j = 1,\ 2, \ldots, J \tag{23}$$

and $\mathbb{I}$ is the identity matrix.

To solve the non-linear problem, an incremental procedure is used, with prescribed steps of applied action (axial force N or displacement ΔL). The solution for the general step is obtained iteratively by updating the secant stiffnesses. A relaxation coefficient is also introduced when strong non-linearities may cause problem in the convergence of the method.

The system in Equation 21 is solved by means of the iterative biconjugate gradient method using as initial guess the solution reached at the previous step. Moreover, as a preconditioner, incomplete LU factorization of $\mathbb{K}$ is adopted.

When the tensile stress in concrete reaches the strength f_{ct} in the j-th node, a transverse crack in concrete arises. The crack produces relative displacement in concrete between two subsequent nodes, while continuity is prescribed for steel and FRP-plates. This condition is introduced substituting the j-th row in Equation 21 by suitable internal boundary conditions:

$$\mathbb{B}_c\,\mathbf{y}_j + \mathbb{B}_d\,\mathbf{y}_{j+1} = \mathfrak{a}_j(w), \tag{24}$$

where the crack width $w = u_{c,j+1} - u_{c,j}$ is the difference of axial displacements in concrete between two contiguous nodes.

5 AN ILLUSTRATIVE NUMERICAL EXAMPLE

A displacement-controlled test on a R/C tensile member strengthened by two FRP plates has been numerically simulated. Geometry and material properties of the specimen are reported in Figure 5.

The numerical analysis has been performed by prescribing an increasing displacement at the right end of the reinforcing steel bars, with displacement steps equal to 0.02 mm.

The displacement-force $\Delta L - N$ curve obtained from the analysis is represented with a solid line in Figure 6.

For $\Delta L = 0.38$ mm, tensile stress σ_c reaches concrete strength f_{ct} in a wide central portion, where a transverse crack may theoretically occur.

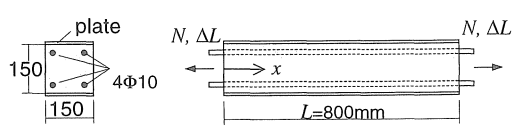

CONCRETE	$A_c = 150 \times 150$ mm^2	$E_c = 33640$ N/mm^2
	$f_c = 36.4$ N/mm^2	$f_{ct} = 3.64$ N/mm^2
STEEL	$A_s = 3.14$ mm^2	$E_s = 200000$ N/mm^2
PLATE	$b_p = 150$ mm	$h_p = 1.016$ mm
	$E_p = 108380$ N/mm^2	

Figure 5. R/C tensile member strengthened by FRP-plates: geometry and mechanical properties.

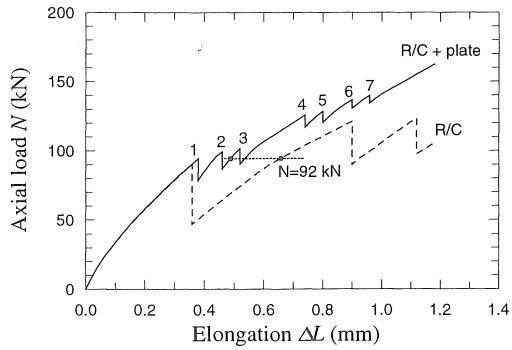

Figure 6. Comparison between plated and unplated R/C tensile members: axial load – elongation curves.

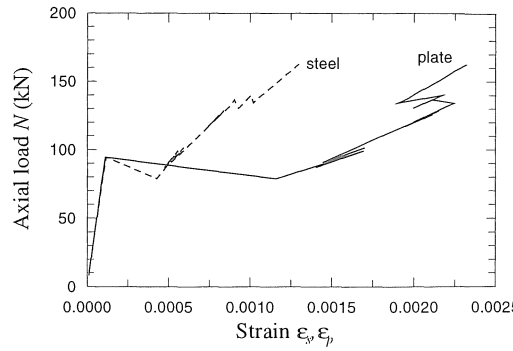

Figure 8. Axial load–strain curves: comparison between plate and steel strains in section at x=400 mm, where first crack in concrete occurs.

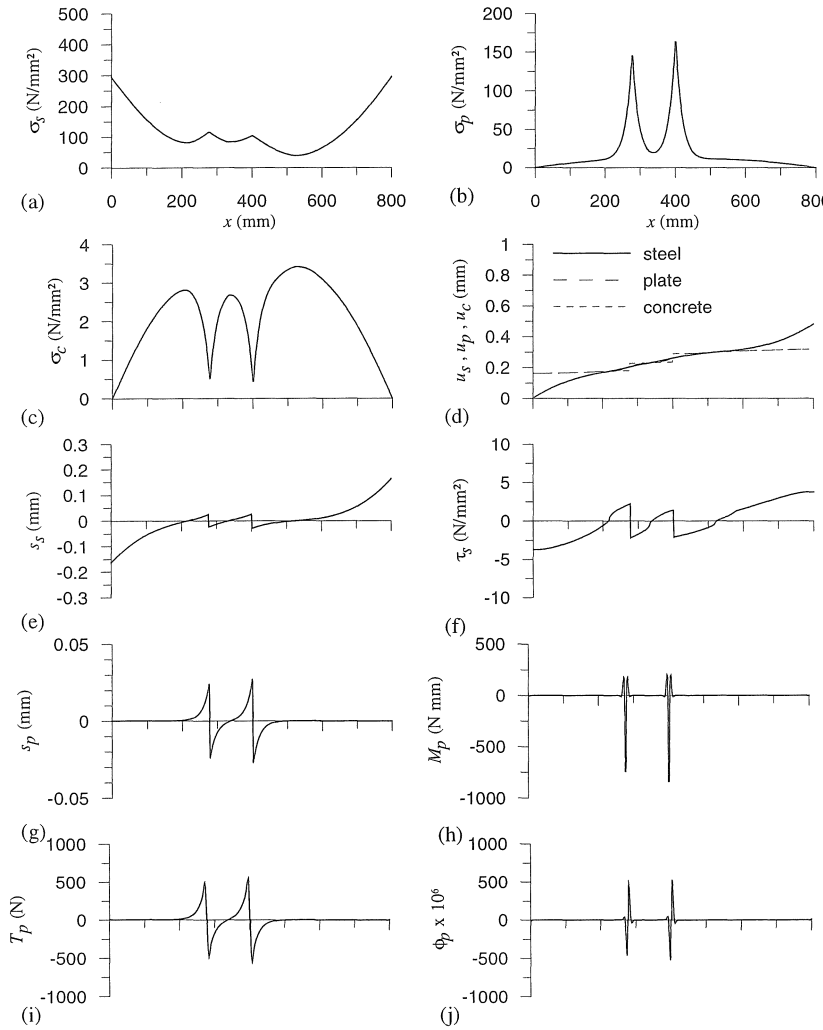

Figure 7 – Distribution of kinematic and static unknowns along the specimen, obtained for $\Delta L = 0.5$ mm (two cracks): (a) steel stress; (b) plate stress; (c) concrete stress; (d) displacements; (e) steel slip; (f) bond stress between steel and concrete; (g) FRP-plate slip; (h) bending moment in plate; (i) shear in plate; (j) rotation of plate.

In fact, since the member is longer than twice the transmission length of bond stresses, in the central portion stresses in steel, plate and concrete are constant and correspond to stage I hypothesis (perfect bond between materials). Within the zone of maximum constant stresses, the exact position of the crack cannot be determined, since it depends on material heterogeneities, as already discussed in details in Fantilli et al. (1998).

In the present analysis, the onset of the first transverse crack has been chosen in the middle of the specimen ($x = 400$ mm).

Crack formation causes a discontinuity in $\Delta L - N$ diagram, which is revealed by an unstable vertical path (point 1 in Figure 6). As a consequence, the reduction of applied load N produces unloading which justifies the adoption of cyclic relationships for concrete in tension and steel-concrete interface law.

Increasing the elongation ΔL, more cracks arise along the member. The evolution of the crack pattern is documented by the zigzag path in Figure 6.

The distributions of all the statical and kinematic unknowns along the specimen obtained for $\Delta L = 0.5$ mm are reported in Figure 7. In particular, Figure 7a shows that plates reduce steel stress σ_s around the cracks, which is almost uniform and smaller than at the edges. On the contrary, significant plate stress σ_p are present in cracked sections, much greater than those that can be found in the no-cracked portions of the member close to plate ends (Figure 7b). The jumps in displacement (Figure 7d) and slip (Figures 7e, f) curves indicate crack width. Due to small crack width, cohesive tensile stresses across the cracked sections are important and must be considered (Figure 7c).

Figure 8 shows the evolution of steel and plate strains in the cracked cross section in the middle of the specimen. It is clearly confirmed that in the cracked section classical stage II hypothesis (i.e. same strain in reinforcing bars and composite plates) does not apply. In particular, strains in composite plates are greater than in steel bars. The ratio between strains is about $\varepsilon_p / \varepsilon_s = 3.0$ after the formation of first crack, and about $\varepsilon_p / \varepsilon_s = 1.85$ at the formation of the last crack.

Finally, the behavior of the plated tensile member has been compared with the correspondent unstrengthened counterpart. The elongation-force diagram (Figure 6) shows that no significant differences can be noted before the first crack (plates do not contribute significantly to stiffness increase), which occurs approximately at the same elongation level. After cracking, a smaller number of large cracks can be noted in the unplated case, resulting in an axial elongation about 40% larger. The stress distributions and axial displacement for steel and concrete and steel-concrete slip for the unstrengthened (dashed line) and the strengthened case (solid line) are compared in Figure 9, for $N = 92$ kN. It can be noted that

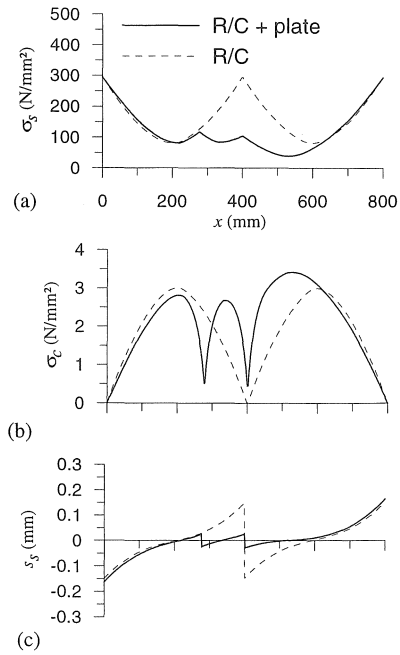

Figure 9. Comparison between plated and unplated R/C tensile members ($N = 92$ kN): (a) steel stress; (b) concrete stress; (c) slip between steel and concrete.

the stress in steel, the steel-concrete slip and the crack width are significantly larger for the unplated case in the cracked region, whereas the solution are almost coincident in the uncracked zones close to member extremities. For instance, the width of the central crack is around 0.3 mm for the unplated member and 0.05 mm for the plated one.

ACKNOWLEDGEMENT

The financial support of the Ministry of the University and Scientific and Technological Research (MURST-60%) is gratefully acknowledged.

REFERENCES

Ascher, U.M., Mattheij, R.M.M. & Russel, R.D. 1988. *Numerical Solution of Boundary Value Problems for Ordinary Differential Equations.* New Jersey: Prentice Hall, Englewood Cliffs.

Bresson, J. 1971. Nouvelles recherches et applications concernant l'utilisation des collages dans les structures. *Beton Plaque Annales de l'Institut Technique* 278.

Brosens, K. & van Gemert, D. 1998. Plate end shear design for external CFRP laminates. In *FRAMCOS-3, Freiburg, Germany*: 1793-1804.

CEB-FIP 1992. Model Code 1990, Bulletin d'Information n. 230. London: Tomas Telford.

Chajes, M.J., Finch, W.W. jr., Januska, T.F., & Thomson, T.A. jr. 1996. Bond and force transfer of composite material plates bonded to concrete. *ACI Structural Journal* 93(2): 208-217.

Eligehausen, R., Bertero V.V., Popov, E.P. 1983. Local bond stress-slip relationship of deformed bars under generalised excitations. *Earthquake Engineering Research Center, Report UCB/EERC*: 83-19.

Fantilli, A.P., Ferretti, D., Iori, I. & Vallini, P. 1998. Flexural deformability of reinforced concrete beams. *J. of Structural Engineering ASCE* 124(9): 1041-1049.

Ferretti, D. & Savoia, M. 2000. Serviceability behavior of r/c tensile members strengthened by FRP plates, *Studi e Ricerche* 21 (to appear).

FIB TG 4.2 1999. Bond of Continuous Fibre Sheets and Plates, FIB, Working Party 7, Preliminary Report.

Garden, H.N., Quantrill, R.J., Hollaway, L.C., Thorne, A.M. & Parke, G.A.R. 1998. An experimental study of the anchorage length of carbon fibre composite plates used to strengthen r.c. beams. *Constr. Build. Materials* 12: 203-219.

Hankers, Ch. 1995. *Zum Verbundverhalten Laschenverstarkter Betonbautelie unter nicht Vorwiegend RuhenderBeanspruchung.* PhD Dissertation, TU Braunschweig.

Hankers, C. & Rostasy, F.S. 1997. Verbundtragverhalten laschenverstarker Betonbautele unter schwellender Verbundbeanspruchung. *Beton und Stahlbetonbau* 92: 19-23.

Hordijk, D.A. 1992. *Local approach to fatigue of concrete.* PhD Thesis, Delft.

Jansze, W. 1997. *Strengthening of reinforced concrete members in bending by externally bonded steel plates.* PhD Thesis, Delft.

Jones, R., Swamy, R.N. & Charif, A. 1988. Plate separation and anchorage of reinforced concrete beams strengthened by epoxy-bonded steel plates. *The Structural Engineer* 66: 85-94 and 187-188.

JSCE (Machida A. Ed.) 1997. Recommendation for Design and Construction of Concrete Structures using Continuous Fiber Reinforcing Materials, Research Committee on Continuous Fiber Reinforcing Materials.

Lee, Y.J., Boothby, T.E., Bakis, C.E. & Nanni, A. 1999. Slip modulus of FRP sheets bonded to concrete. *J. of Composites for Construction ASCE* 3(4): 161-167.

Malek, A.M., Saadatmanesh, H. & Ehsani, M.R. 1998. Prediction of failure load of R/C beams strengthened with FRP plate due to stress concentration at the plate end. *ACI Structural Journal* 95: 142-152.

Nanni, A. 1993. Flexural behavior and design of RC members using FRP reinforcement. *J. of Structural Engineering ASCE* 119(11): 3344-3359.

Ranisch, E.H. 1982. Zur Tragfahigkeit von Verklebungen zwischen Baustahl und Beton – Geklebte Bewehrung. Heft 54, IBMB, Braunschweig.

Roberts, T.M. 1989a. Approximate analysis of shear and normal stress concentrations in the adhesive layer of plated RC-beams. *The Structural Engineer* 67(12): 229-233.

Roberts, T.M. 1989b. Shear and normal stresses in adhesive joints. *J. Engineering Mechanics ASCE* 115(11): 2460-2476.

Saadatmanesh, H. & Ehsani, M.R. 1991. RC beams strengthened with GFRP plates. I: Experimental study; II: Analysis and parametrical study. *J. of Structural Engineering ASCE* 117(11): 3417-3433 and 3434-3455.

Sato, Y., Shouji, K., Ueda, T. & Kakuta, Y. 1999. Uniaxial tensile behavior of reinforced concrete elements strengthened by carbon fiber sheets. In *Fourth International Symposium on Fiber Reinforced Polymer Reinforcement for Reinforced Concrete Structures*, ACI SP-188, eds. Dolan, Rizkalla & Nanni: 697-710.

Swamy, R.N., Jones, R. & Charif, A. 1986. Shear adhesion properties of epoxy resin adhesives. In *Int. Symp. on Adhesion between Polymers and Concrete*: 741-755.

Taljsten, B. 1997a. Strengthening of beams by plate bonding. *J. of Materials in Civil Engineering* 9(4): 206-211.

Taljsten, B. 1997b. Defining anchor lengths of steel and CFRP plates bonded to concrete. *Int. J. of Adhesion and Adhesives*. 17(4): 319-327.

Tripi, J.M., Bakis, C.E., Boothby, T.E. & Nanni, A. 2000. Deformation in concrete with external CFRP sheet reinforcement. *Journal of Composites for Construction* 4(2): 85-94.

Varastehpour, H. & Hamelin, P. 1997. Strengthening of concrete beams using fiber-reinforced plastics. *Materials and Structures* 30: 160-166.

Volkersen, O. 1938. Die Nietkraftverteilung in zugbeanspruchenden Nietverbindungen mit Konstanten Laschenquerschnitten. *Luftfahrtforschung* 15:41-47.

Volnyy, V.A. & Pantelides, Ch. P. 1999. Bond length of CFRP composites attached to precast concrete walls. *J. of Composites for Construction ASCE* 3(4): 168-176.

Ziraba, Y.N., Baluch, M.H., Basunbul, I.A., Azad, A.K., Al-Sulaimani, G.J. & Sharif, A.M. 1995. Combined experimental-numerical approach to characterization of steel-glue-concrete interface. *Materials and Structures* 28: 518-525.